IMAGING METHODOLOGY – Communication

Magnetic Resonance in Medicine 66:950–956 (2011)

Spatially Encoded Phase-Contrast MRI—3D MRI Movies of 1D and 2D Structures at Millisecond Resolution

Klaus-Dietmar Merboldt, Martin Uecker, Dirk Voit, and Jens Frahm*

This work demonstrates that the principles underlying phase-contrast MRI may be used to encode spatial rather than flow information along a perpendicular dimension, if this dimension contains an MRI-visible object at only one spatial location. In particular, the situation applies to 3D mapping of curved 2D structures which requires only two projection images with different spatial phase-encoding gradients. These phase-contrast gradients define the field of view and mean spin-density positions of the object in the perpendicular dimension by respective phase differences. When combined with highly undersampled radial fast low angle shot (FLASH) and image reconstruction by regularized nonlinear inversion, spatial phase-contrast MRI allows for dynamic 3D mapping of 2D structures in real time. First examples include 3D MRI movies of the acting human hand at a temporal resolution of 50 ms. With an even simpler technique, 3D maps of curved 1D structures may be obtained from only three acquisitions of a frequency-encoded MRI signal with two perpendicular phase encodings. Here, 3D MRI movies of a rapidly rotating banana were obtained at 5 ms resolution or 200 frames per second. In conclusion, spatial phase-contrast 3D MRI of 2D or 1D structures is respective two or four orders of magnitude faster than conventional 3D MRI. Magn Reson Med 66:950–956, 2011. © 2011 Wiley-Liss, Inc.

Key words: 3D MRI; 3D imaging; iterative reconstruction; parallel imaging; phase-contrast imaging; real-time imaging

Phase-contrast MRI is a well established method for dynamically mapping flow velocities which has been developed during the early stages of MRI, e.g., see (1–4). Typically, it is based on the phase difference between two cross-sectional images with different bipolar velocity-encoding gradients. The resulting 3D dataset comprises two spatial dimensions and one velocity (phase difference) dimension, so that each image pixel presents with a unique velocity value. This work demonstrates that the same principle may be used to encode spatial information along the third dimension, i.e., perpendicular to an imaging plane, if this dimension contains only one spatial location and the radiofrequency (RF) excitation covers the entire volume. Instead of applying a self-compensated bipolar gradient with a nulled zero-order moment (i.e., the time integral of the gradient) but a nonvanishing first-order moment (i.e., the time integral of the gradient multiplied with the time) as required for velocity encoding, the proposed method in its simplest form employs two monopolar encoding gradients with a nonvanishing zero-order moment and opposite polarity.

Although spatial phase encoding is at the heart of all Cartesian-based MRI, the use of only two settings for the determination of a phase difference that directly maps the spatial position of an object along a respective orientation does not seem to have attracted attention. Nevertheless, a somewhat related idea has been employed to perform what appears to be a complementary task: rather than mapping all stationary spins of an object in 3D space after nonselective excitation, so-called displacement encoding techniques with stimulated echoes or DENSE (5,6) attempt to characterize all moving spins within a selectively excited cross-section. Pertinent applications therefore focus on the assessment of regional elastic tissue properties or intramyocardial functions.

As proposed here, spatially encoded phase-contrast MRI particularly applies to 3D MRI of curved 2D structures or surface layers that may be mapped by only two projection images with a different degree of perpendicular phase encoding. In fact, if the object represents as a curved linear or 1D structure, the necessary information for a 3D MRI representation may further be reduced to the acquisition of only three frequency-encoded MRI signals with different spatial phase-contrast gradients.

The present work outlines the basic principles of spatial phase-contrast MRI and provides preliminary experimental examples that demonstrate its potential for dynamic 3D MRI of 2D and 1D structures at ultra-high temporal resolution.

MATERIALS AND METHODS

Spatial Phase-Contrast 3D MRI of 2D Structures

Figure 1 shows a schematic RF pulse and magnetic field gradient sequence for spatially encoded phase-contrast MRI. The two repetition intervals (TR) illustrate an implementation for 3D mapping of 2D structures which exploits a radial fast low angle shot (FLASH) MRI sequence for the projection images as described (7). A 3D representation of the object is derived from a phase-contrast projection map which, for example, may be obtained by phase-sensitive reconstructions of the two projection images followed by a pixelwise calculation of respective phase differences. The locations of the object's mean spin densities within the field of view (FOV) of the phase-difference dimension are defined by a numerical value rather than affected by a discrete sampling pattern as in Fourier imaging. Thus, in order to ensure

Biomedizinische NMR Forschungs GmbH am Max-Planck-Institut für biophysikalische Chemie, Göttingen, Germany.

Additional Supporting Information may be found in the online version of this article.

*Correspondence to: Jens Frahm, Professor, Biomedizinische NMR Forschungs GmbH am Max-Planck-Institut für biophysikalische Chemie, 37070 Göttingen, Germany. E-mail: jfrahm@gwdg.de

Received 18 March 2011; revised 29 June 2011; accepted 30 June 2011.

DOI 10.1002/mrm.23114

Published online 12 August 2011 in Wiley Online Library (wileyonlinelibrary.com).

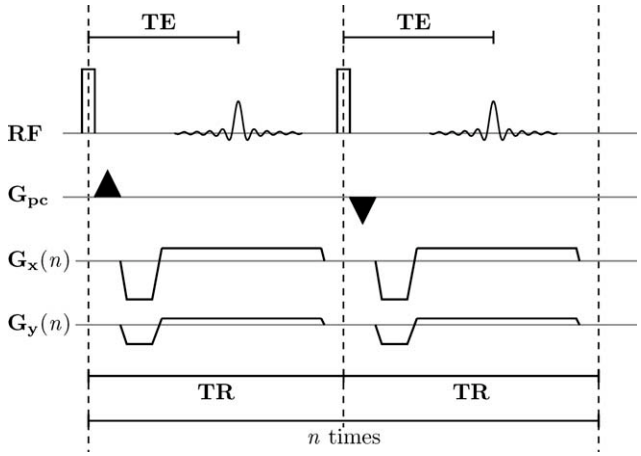

FIG. 1. Schematic diagram for spatially encoded phase-contrast 3D MRI of a 2D object. The example refers to a single-echo radial FLASH implementation (TE = echo time) with two monopolar phase-encoding gradients G_{pc} of opposite sign in alternate repetition intervals TR. The complete acquisition of two phase-encoded projection images (or one phase-contrast projection map) requires n repetitions corresponding to a total measuring time of $2n$ TR. RF = radiofrequency (nonselective excitation), G_x and G_y = frequency-encoding gradients (radial spokes).

adequate positional accuracy of the acquired phase-difference information, the object should be thin and the spatial phase-contrast gradients should be directed along its shortest axis.

When using two monopolar phase-encoding gradients G_{pc} of equal strength but opposite polarity, which in Fig. 1 are applied perpendicular to the 2D radial encoding gradients G_x and G_y, the FOV has maximum extensions of $\pm$FOV/2 that correspond to phases of $\pm\pi$ according to

$$2\pi = \gamma\,\mathrm{FOV}\,M_0(G_{pc})$$

with γ the gyromagnetic ratio and $M_0(G_{pc})$ the zero-order moment (i.e., time integral) of the phase-contrast gradient G_{pc}. The 3D position of each pixel in the phase-contrast projection map is given by its phase-difference value relative to the phase value of the FOV which in this case would be $\pm\ \pi$. This definition of an unaliased spatial FOV is in complete analogy to the selection of a maximum VENC value in velocity-encoded phase-contrast MRI.

In contrast to velocity-encoding gradients, however, a pair of spatial phase-contrast gradients comprises at least one gradient with a nonvanishing zero-order moment. While the present results were obtained with two monopolar gradients of opposite polarity, the implementation of a sequence with only one spatial phase-encoding gradient for one image and no phase encoding for the other turned out to be technically equivalent. Moreover, in the version shown in Fig. 1, the (typically small) phase-encoding gradients are applied in an interleaved manner, that is in successive repetition intervals TR. However, also sequential acquisitions of complete images with different phase encodings have been realized and tested to yield the same image quality. Such strategies may be exploited for sliding-window reconstructions of phase-difference maps at twice the frame rate. Finally, the actual sequence design also allows for a replacement of the nonselective RF excitation by a spatially selective or chemical shift-selective RF excitation.

Dynamic 3D MRI of 2D Structures

In order to dynamically visualize curved surface structures in 3D space at high speed, the radial encoding of the spatially-encoded phase-contrast images is realized with pronounced undersampling. Several approaches have been proposed to deal with the respective reconstruction problem, for example see (8–12). Here, image reconstructions are accomplished with the use of a regularized nonlinear inversion algorithm as recently developed for improved parallel MRI (13) with radial encodings (14) at ultra-high temporal resolution (15,16). Because these reconstructions are performed offline due to the high computational demand of the iterative algorithm, online monitoring of the magnitude images in real time is accomplished by gridding of more complete datasets which may be obtained by combining several (typically five) successively acquired datasets with complementary radial encodings (7).

It should be noted that the proposed inverse reconstruction successfully applies parallel imaging in 3D space by using only 2D coil sensitivity maps. The effective sensitivities are projections of the physical 3D coil sensitivities along the 2D structure onto the chosen imaging plane. For a surface structure moving in 3D space this projection may rapidly change in time, which requires a continuous estimation of the coil sensitivities as ensured by the chosen nonlinear inverse algorithm (13–15). To avoid phase errors due to varying coil sensitivities, each reconstructed image is first multiplied with its jointly estimated sensitivities to obtain a separate image for each channel. The background phase from off-resonance effects and coil sensitivities is removed when computing the respective phase differences. Finally, the phase-contrast maps from all channels are combined by weighting each pixel with its energy in the magnitude image of the respective channel.

Spatial Phase-Contrast 3D MRI of 1D Structures

A technically much simpler variant of spatially encoded phase-contrast MRI refers to 3D MRI of a curved 1D object or linear structure arranged in 3D space. The approach allows for even faster acquisitions and reconstructions than required for measurements of a 2D object. In fact, as shown in Fig. 2, the basic experiment reduces to the acquisition of only three frequency-encoded MRI signals with two perpendicular spatial phase-encoding gradients. Accordingly, 3D reconstructions of the 1D object may directly be obtained by three 1D Fourier transformations and the calculation of only two phase-difference vectors.

3D mapping of a curved 1D object involves one frequency-encoded dimension and two spatial phase-difference dimensions and may be accomplished within a measuring time of 3 TR. In this work, real-time 3D MRI of 1D structures was performed by rapid FLASH

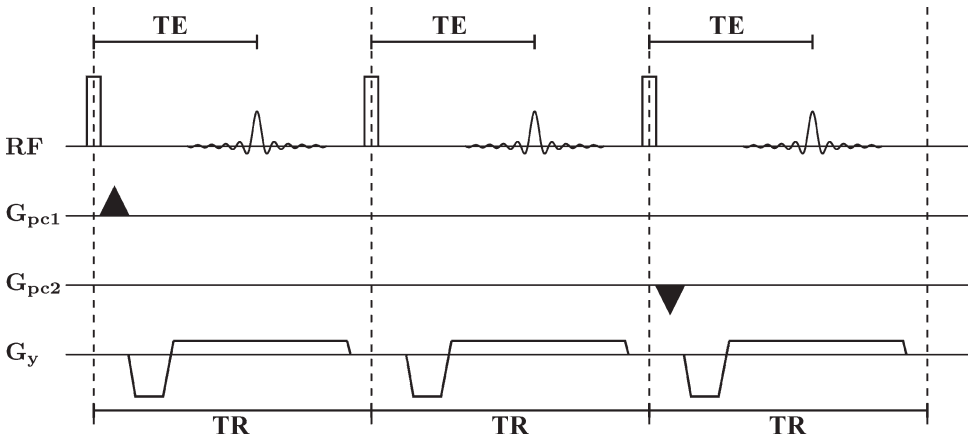

FIG. 2. Schematic diagram for spatially encoded phase-contrast 3D MRI of a 1D object. The example refers to the acquisition of three frequency-encoded gradient echoes with two perpendicular phase-encoding gradients G_{pc1} and G_{pc2}. The complete acquisition corresponds to a total measuring time of 3 TR.

acquisitions of differently phase-encoded short-echo time (short-TE) gradient echoes within three successive short-TR intervals. The current implementation employed frequency-encoded lines with two perpendicular phase-encoding gradients and one reference without spatial phase encoding. Again, other combinations of spatial phase-contrast gradients are possible as well.

Finally, some information about the "thickness" of a 1D object in spatial phase-contrast MRI is available from the amplitude information of the individual projections. Similar arguments hold true for 3D MRI of 2D objects and the amplitudes of the corresponding projection images. Although this information includes heterogeneous differences in relaxation-weighted spin density, it may be used to dynamically assign a "thickness" to the 3D reconstruction that retains relative differences within the object. In any case, it is more important to choose a large FOV along a phase-difference dimension in order to let the object appear relatively "thin" despite its true thickness. This also reduces the risk for positional aliasing during movement of the object.

Phantom and Human MRI Studies

All studies were performed at 3 T (TIM Trio, Siemens Healthcare, Erlangen, Germany) with the use of a standard 32-channel head coil. As depicted in Fig. 1 the current implementation of spatial phase-contrast MRI employed a RF-spoiled radial FLASH sequence with nonselective RF excitation and either an interleaved (every other TR) or sequential scheme (every other image) for spatial phase encoding. The FOV in the phase-difference dimension varied from 128 mm (phantom studies) to 256 mm (human studies). Moreover, in this first study, all acquisitions were based on spatial phase-contrast gradients with a monopolar waveform as illustrated in Figs. 1 and 2.

Different phantoms of a tube filled with doped water (reduced T1 relaxation time) served to demonstrate the principles of spatial phase-contrast MRI. Respective images (flip angle 12°) were acquired using an interleaved encoding scheme and full *k*-space sampling at 1.0 mm linear resolution (minimum TR/TE = 2.00/1.32 ms). These images were reconstructed by a conventional gridding algorithm comprising a density compensation, convolution with a Kaiser-Bessel kernel, interpolation to a rectangular grid, inverse fast fourier transformation (FFT) and roll-off correction compensating for the interpolation in k space (7).

3D MRI movies of a linear structure were obtained from a rapidly rotating banana hanging in the head coil on a twisted rubber band. Immediately before scanning the rubber band was manually released. Respective movies (flip angle 6°) had a linear resolution of 2.0 mm and a temporal resolution of 5.0 ms yielding 200 frames per second (minimum TR/TE = 1.68/1.15 ms for moderate gradient switching times).

Three healthy subjects participated in studies of hand and finger movements that correspond to dynamic 3D MRI of a 2D structure. All subjects gave informed written consent before each examination. Human studies were performed with the use of a dual-echo radial FLASH MRI version as previously developed for cardiovascular real-time MRI (16). Pertinent applications result in the simultaneous recording of two 2D phase-contrast maps under opposed-phase and in-phase conditions for water/fat signal contributions, respectively. Their complementary phase information was exploited to improve respective 3D representations. The acquisition parameters for strongly undersampled images (TR = 2.86 ms, TE1/TE2 = 1.25/2.25 ms, flip angle 3°, 2.0 mm in-plane resolution) achieved real-time 3D MRI movies with a minimum measuring time of 25 ms per image (9 spokes) or 50 ms per phase-difference map. These applications employed a sequential acquisition strategy of two phase-encoded images with opposite polarity. The reconstruction of all undersampled images relied on regularized nonlinear inversion (13–15).

Translation of the phase-contrast information into a spatial location and multi-dimensional visualization was accomplished using routines written in MATLAB (MathWorks, Natick, MA). Because the spatial phase information is given as a single numerical value, its 3D visualization as a voxel is realized by assigning the position an arbitrary though reasonable "thickness" which corresponds to the signal amplitude of the respective magnitude information. Together with the choice of a minimum intensity threshold, the procedure effectively eliminates noise contributions and maintains gross structural differences within the object under investigation. In some cases, the visualization of a 3D movement was improved by adding an artificial shadow to the reconstructed object.

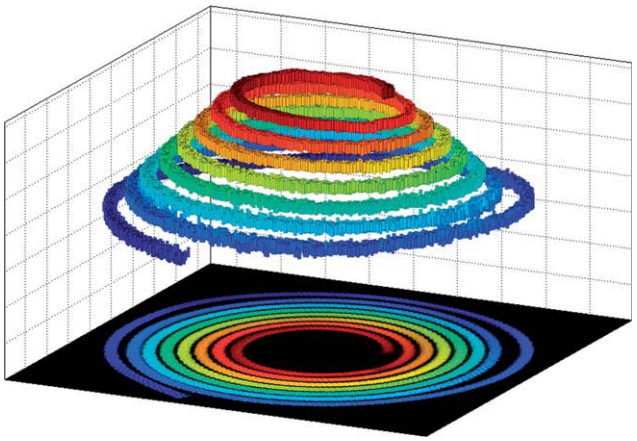

FIG. 3. Spatial phase-contrast 3D MRI of a water-filled tube arranged as a 3D spiral (fully sampled radial FLASH with gridding reconstruction). (Top) 3D representation and (bottom) corresponding 2D phase-contrast projection map (magnitude image with color-coded overlay of phase differences: blue to yellow to red). The data were acquired with the sequence shown in Fig. 1. Other parameters: flip angle 12°, TR/TE = 2.35/1.61 ms, 1.0 mm in-plane resolution. [Color figure can be viewed in the online issue, which is available at wileyonlinelibrary.com.]

RESULTS

Spatial Phase-Contrast 3D MRI of 2D Structures

The principle of spatially encoded phase-contrast MRI is illustrated in Fig. 3 which depicts a water-filled tube arranged as a 3D spiral. The corresponding 2D phase-contrast projection map, that is the phase difference of two spatially phase-encoded 2D projection images, is visualized as a magnitude image with color-coded overlay of phase differences (Fig. 3, bottom) and as a 3D view after translation of the phase information into a spatial dimension (Fig. 3, top).

Figure 4 presents the basic results of a spatially encoded phase-contrast MRI study of the human hand recorded with strongly undersampled dual-echo radial FLASH. The magnitude images with color-coded phase overlay demonstrate that the phase information in the in vivo situation is dominated by magnetic field inhomogeneities and water/fat chemical shift differences in both opposed-phase and in-phase images (Fig. 4a,b). These effects cancel in the corresponding phase-contrast maps (Fig. 4c), whereas phase differences due to the spatial encoding are retained. It also turns out that the opposed-phase situation may lead to regions of low intensities, for example, due to bone marrow (Fig. 4, top), while the in-phase situation offers a more contiguous signal support for a reliable phase-contrast information in as many pixels as possible (Fig. 4, bottom). However, because both maps provide useful complementary information, the chosen visualization strategy took advantage of all information by combining the in-phase magnitude images with the best defined phase value per pixel in either phase-contrast map. The resulting map was then translated into a 3D representation.

A corresponding dynamic study of the human hand and fingers is depicted in Fig. 5 which shows a series of selected 3D representations and original phase-difference

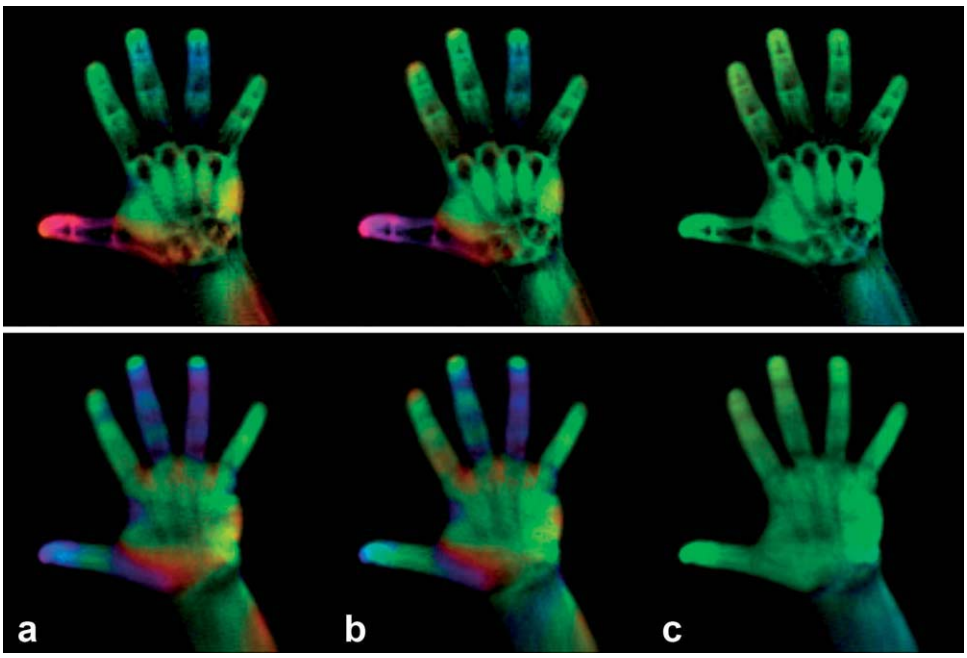

FIG. 4. Spatial phase-contrast MRI of the human hand (undersampled dual-echo radial FLASH with image reconstruction by regularized nonlinear inversion). (Top) Opposed-phase and (bottom) in-phase condition for water/fat signals, (**a,b**) pair of spatially phase-encoded projection images with color-coded overlay of the absolute phase, (**c**) corresponding 2D phase-contrast projection maps representing the differential spatial encoding. Other parameters: nonselective RF excitation, flip angle 3°, sequential phase-encoding in alternate images, TR = 2.86 ms, TE1/TE2 = 1.25/2.25 ms, 2.0 mm in-plane resolution. The acquisition of 9 spokes per image resulted in a measuring time of 25 ms per image and 50 ms per phase-contrast map. [Color figure can be viewed in the online issue, which is available at wileyonlinelibrary.com.]

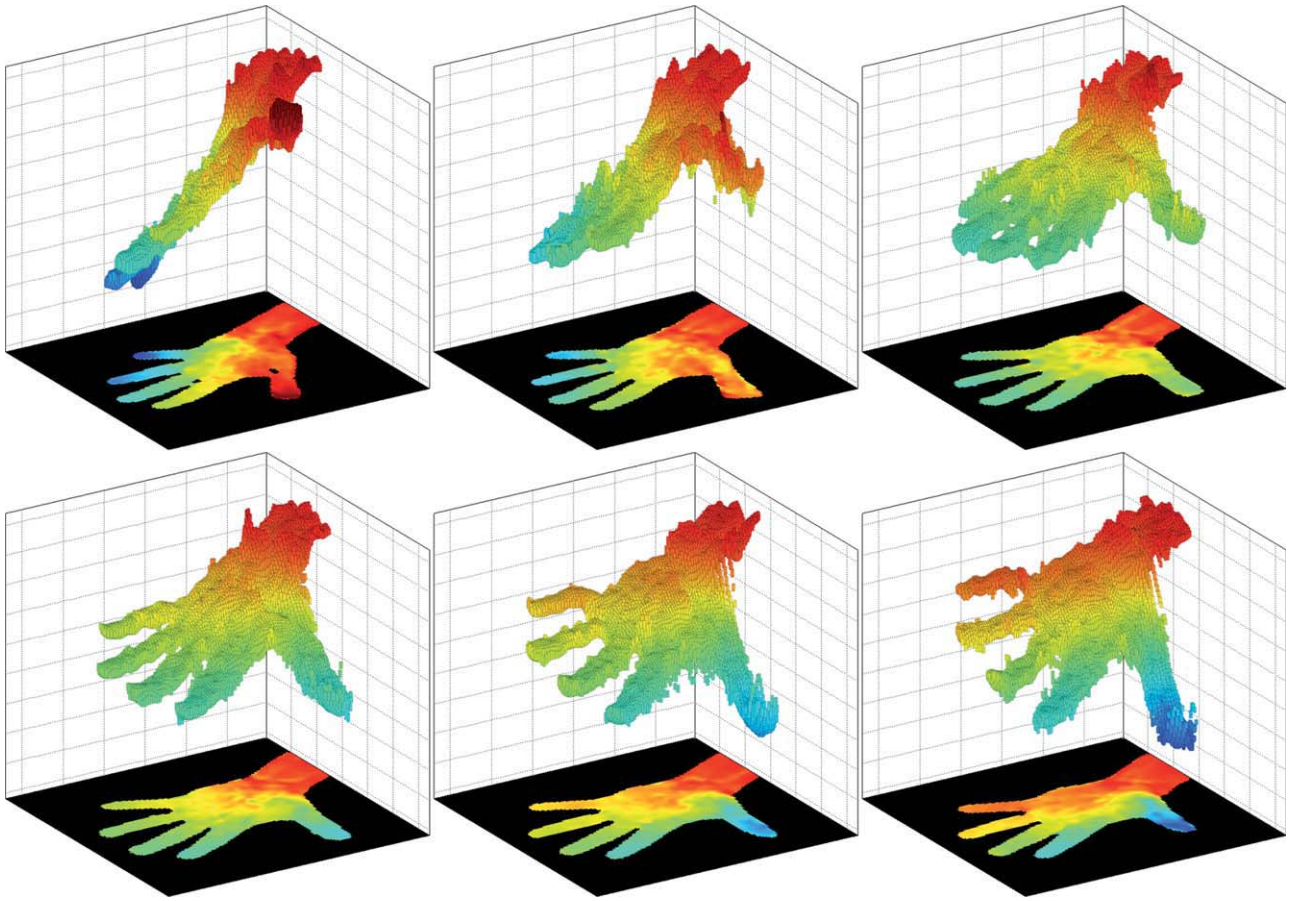

FIG. 5. Consecutive 3D representations of a spatial phase-contrast 3D MRI movie and original 2D phase-contrast projection maps (bottom plane) of a moving human hand at a temporal resolution of 50 ms (same data and parameters as in Fig. 4). The images (top left to bottom right) depict every 3rd frame (every 150 ms) covering a 800 ms period from a longer movie (Supporting Information 1). [Color figure can be viewed in the online issue, which is available at wileyonlinelibrary.com.]

maps (bottom plane) visualizing movements in 3D space at a temporal resolution of 50 ms. The acquisition was based on a dual-echo FLASH sequence and the reconstruction employed the combined phase-contrast maps as outlined above. The full movie is available as Supporting Information 1.

Spatial Phase-Contrast 3D MRI of 1D Structures

As illustrated in Fig. 2, three acquisitions of a frequency-encoded MRI signal with suitable phase-contrast gradients are sufficient for 3D mapping of a water-filled tube with 3D curvature. Figure 6 shows a corresponding example obtained within a measuring time of only 6.0 ms (3 TR). A similar experiment with a straight linear tube served to estimate the positional accuracy of this particular phase-contrast MRI scenario which might be expected to represent a worst case because of its very limited signal-to-noise ratio. Based on the respective phase differences along the tube, the standard deviation of the numerical values yielded 1.2% of the chosen FOV (corresponding to 2 π). In other words, for a FOV of 128 mm along the phase-difference dimension, the spatial accuracy resulted in a standard deviation of 1.5 mm.

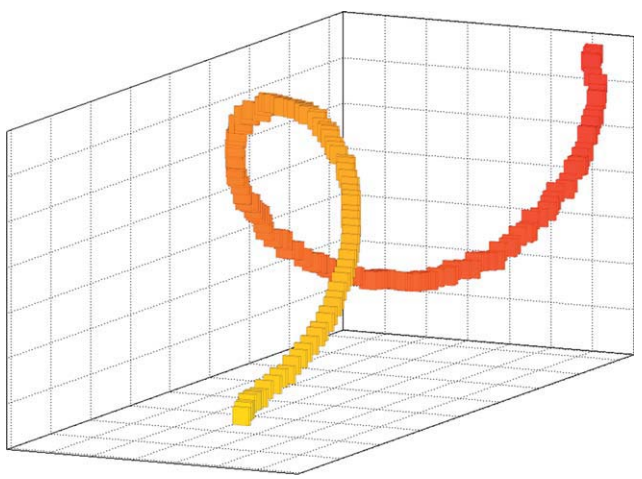

FIG. 6. Spatial phase-contrast 3D MRI of a water-filled tube with 3D curvature (frequency-encoded gradient echo with reconstruction by Fourier transformation). The 3D representation is based on data acquired within a total measuring time of 6.0 ms using the sequence shown in Fig. 2. Other parameters: flip angle 12°, TR/TE = 2.00/1.32 ms, 1.0 mm linear resolution. The color only serves to better visualize spatial depth. [Color figure can be viewed in the online issue, which is available at wileyonlinelibrary.com.]

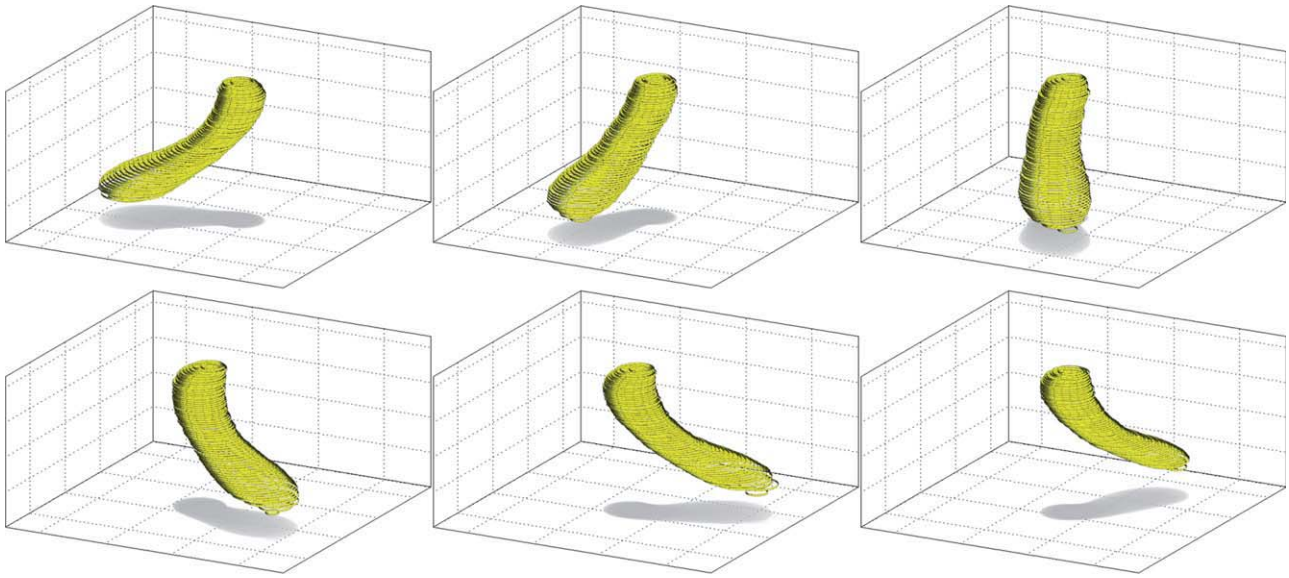

FIG. 7. Consecutive 3D representations of a spatial phase-contrast 3D MRI movie of a rotating banana at a temporal resolution of 5.0 ms. The data were acquired with the sequence shown in Fig. 2. Other parameters: flip angle 6°, TR/TE = 1.68/1.15 ms, 2.0 mm linear resolution, artificial shading. The images (top left to bottom right) depict every 20th frame (every 100 ms) covering a 505 ms period from a longer movie (Supporting Information 2). [Color figure can be viewed in the online issue, which is available at wileyonlinelibrary.com.]

A dynamic study of a rapidly moving linear object is shown in Fig. 7 presenting selected views of a rotating banana after release from a twisted rubber band fixed at its top end. The corresponding 3D MRI movie achieved a temporal resolution of 5.0 ms, that is 200 frames per second, and is available as Supporting Information 2.

DISCUSSION

To the best of our knowledge this appears to be the first report of spatially encoded phase-contrast MRI and its application to 3D mapping of static or dynamic objects. When imaging curved 2D structures or surface layers in 3D space, the proposed method reduces the dimension of the necessary MRI experiment from three to two, which accelerates the acquisition by two orders of magnitude in comparison to conventional 3D MRI. Furthermore, for 3D studies of linear structures the measuring time is reduced from typically 128 (to 256) $\times$ 256 $\times$ TR to only 3 TR, that is by four orders of magnitude.

Here, we obtained 3D MRI movies of the human hand at a temporal resolution of 50 ms using dual-echo radial FLASH with pronounced undersampling and image reconstruction by nonlinear inversion. The concept of spatial phase-contrast MRI was then extended to dynamic 3D MRI of a curved 1D object at a temporal resolution of 5.0 ms. Because the latter experiment relies on only three frequency-encoded MRI signals with different spatial phase encodings, respective 3D reconstructions require only three Fourier transformations and two corresponding phase-difference calculations. Pertinent computations are extremely fast and may immediately be implemented on existing MRI systems for real-time 3D visualization of dynamic linear objects. In this context, it is worth mentioning that—apart from applications to a pure point source—navigator-based techniques are not able to provide the same information as obtained here, that is a 3D spatial location for every pixel of a projection image. For example, even when using a full navigator image perpendicular to a projection image of a 2D object in 3D space, this will only yield 3D information along a single line of pixels (corresponding to the slice thickness of the navigator image), whereas the proposed method fully covers the object's 3D extension with just two spatially phase-encoded projection images that define a spatial phase-contrast projection map.

The phase-difference information in spatial phase-contrast MRI turns out to be rather stable and translates into adequate spatial positions (e.g., see Figs. 3 and 6). Without doubt this phase stability benefits from the use of difference values that largely cancel the effects of static magnetic field inhomogeneities or coil sensitivities or water/fat contributions (e.g., see Fig. 4) in very much the same way as known from velocity-encoded phase-contrast MRI. On the other hand, the spatial accuracy of the method along the phase-difference dimension may suffer from partial volume effects of the projection maps that need to be considered in practical applications. This limitation holds true for objects that are neither thin nor homogeneous along the phase-difference dimension. It is caused by both an amplitude and phase problem: the local signal strength depends on the internal distribution of spin densities and respective relaxation times, and the definition of a spatial position may be compromised by the vectorial calculation of a "mean" phase-difference value from multiple spins. This latter problem is well known in velocity-encoded phase-contrast MRI and has been detailed for quantitative flow measurements (17).

Finally, the present implementation of monopolar spatial phase-contrast gradients may be compromised by very rapidly moving objects that are fast enough to yield additional velocity-dependent phase shifts for short-TE

gradient echoes. Similar to conventional Fourier imaging with Cartesian phase encoding, such unwanted phases will lead to incorrect spatial information along the respective dimension. Here, this phenomenon may have contributed to some spatial inconsistencies for the fast moving thumb as seen in the hand movie at 50 ms resolution (Fig. 5 bottom right and Supporting Information 1). Based on this experience, it is generally recommended to employ velocity-compensated gradient waveforms for spatial phase-contrast MRI. This may be achieved by spatial phase-encoding gradients with an asymmetric bipolar waveform that yield a zero-order moment $M_0(G_{pc}) > 0$ but a first-order moment $M_1(G_{pc}) = 0$.

Although the current "3D of 2D" applications involved a radial FLASH sequence, the principle of spatial phase-contrast MRI may be combined with arbitrary MRI sequences. Possible applications comprise techniques based on spin echoes or stimulated echoes as well as combinations with high-speed methods such as echo-planar or spiral imaging. Also FLASH acquisitions may vary and deliver different contrasts or signal strengths depending on the use of RF spoiling, refocusing gradients, or fully balanced gradients. Moreover, applications may adopt other established techniques such as, for example, spatial presaturation or chemical shift selection which in the case of nonselective spatial excitation (compare Figs. 1 and 2) is simply accomplished by direct frequency-selective RF excitation of water or fat protons or any other desirable frequency range. In fact, spatial phase-contrast MRI of mobile 1D or 2D structures as, for example, the inner surfaces of phase-separated fluid mixtures and their reactions to external forces, may be applied to arbitrary materials regardless of whether they are dense or optically nontransparent or contain MRI-detectable protons at all. In either case, a solution would be to add a "surface contrast" which may be constructed as a flexible (or fluid) layer of mobile protons—if necessary—with a resonance frequency different from water and fat. Suitable aqueous solutions with a lanthanide shift reagent are well-known in NMR spectroscopy and generally available. Alternatively, one may also take advantage of nonproton nuclei as, for example, 19-fluorine, in which case the "surface contrast" may be delivered by perfluorocarbon compounds that are safely used as oxygen carriers in artificial blood substitutes. Another application of spatial phase-contrast MRI will be in interventional MRI, where high-speed 3D visualization of a suitably marked biopsy needle or catheter may be accomplished within a few milliseconds—possibly interleaved with real-time anatomical MRI (15,16). Extending navigator-type or projection studies that rely on the labeling of only a single point (e.g., the tip of a needle), the present method will allow for more spatially complex markers that may help to directly indicate the direction of a moving surgical instrument.

In summary, spatial phase-contrast MRI, and in particular high-speed 3D MRI of dynamic 1D and 2D structures, is expected to find specific applications in physics, chemistry, biology, and medicine as well as in technical research and industry. A variety of sequence versions and methods is foreseeable.

REFERENCES

1. Moran PR. A flow velocity zeugmatographic interlace for NMR imaging in humans. Magn Reson Imaging 1982;1:197–203.
2. Van Dijk P. Direct cardiac NMR imaging of heart wall and blood flow velocity. J Comput Assist Tomogr 1984;8:429–436.
3. Bryant DJ, Payne JA, Firmin DN, Longmore DB. Measurement of flow with NMR imaging using a gradient pulse and phase difference technique. J Comput Assist Tomogr 1984;8:588–593.
4. Nayler GL, Firmin DN, Longmore DB. Blood flow imaging by cine magnetic resonance imaging. J Comput Assist Tomogr 1986;10: 715–722.
5. Chenevert TL, Skovoroda AR, O'Donnell M, Emelianov SY. Elasticity reconstructive imaging by means of stimulated echo MRI. Magn Reson Med 1998;39:482–490.
6. Aletras AH, Ding S, Balaban RS, Wen H. DENSE: displacement encoding with stimulated echoes in cardiac functional MRI. J Magn Reson 1999;137:247–252.
7. Zhang S, Block KT, Frahm J. Magnetic resonance imaging in real time—advances using radial FLASH. J Magn Reson Imaging 2010;31:101–109.
8. Pruessmann KP, Weiger M, Börnert P, Boesiger P. Advances in sensitivitiy encoding with arbitrary k-space trajectories. Magn Reson Med 2001;46:638–651.
9. Yeh EN, Stuber M, McKenzie CA, Botnar RM, Leiner T, Ohliger MA, Grant AK, Willig-Onwuachi JD, Sodickson DK. Inherently self-calibrating non-Cartesian parallel imaging. Magn Reson Med 2005;54: 1–8.
10. Huang F, Vijayakumar S, Li Y, Hertel S, Reza S, Duensing, GR. Self-calibration method for radial GRAPPA/k-t GRAPPA. Magn Reson Med 2007;57:1075–1085.
11. Arunachalam A, Samsonov A, Block WF. Self-calibrated GRAPPA method for 2D and 3D radial data. Magn Reson Med 2007;57: 931–938.
12. Lustig M, Pauly JM. SPIRiT: iterative self-consistent parallel imaging reconstruction from arbitrary k-space. Magn Reson Med 2010;64: 457–471.
13. Uecker M, Hohage T, Block KT, Frahm J. Image reconstruction by regularized nonlinear inversion—joint estimation of coil sensitivities and image content. Magn Reson Med 2008;60:674–682.
14. Uecker M, Zhang S, Frahm J. Nonlinear inverse reconstruction for real-time MRI of the human heart using undersampled radial FLASH. Magn Reson Med 2010;63:1456–1462.
15. Uecker M, Zhang S, Voit D, Karaus A, Merboldt KD, Frahm J. Real-time MRI at a resolution of 20 ms. NMR Biomed 2010;23:986–994.
16. Zhang S, Uecker M, Voit D, Merboldt KD, Frahm J. Real-time cardiovascular magnetic resonance at high temporal resolution: radial FLASH with nonlinear inverse reconstruction. J Cardiovasc Magn Reson 2010;12:39.
17. Bernstein MA, King KF, Zhou, XJ. Handbook of MRI pulse sequences. Amsterdam: Elsevier; 2004. pp 666–672.